Observation of the $5p_{3/2} \rightarrow 6p_{3/2}$ electric-dipole-forbidden transition in atomic rubidium using optical-optical double-resonance spectroscopy

F. Ponciano-Ojeda,[1] S. Hernández-Gómez,[1] O. López-Hernández,[1] C. Mojica-Casique,[1] R. Colín-Rodríguez,[1] F. Ramírez-Martínez,[1,*] J. Flores-Mijangos,[1] D. Sahagún,[2] R. Jáuregui,[2] and J. Jiménez-Mier[1,†]

[1]*Instituto de Ciencias Nucleares, UNAM, Circuito Exterior, Ciudad Universitaria, 04510 México, D.F., Mexico*

[2]*Instituto de Física, UNAM, Ciudad Universitaria, 04510 México, D.F., Mexico*

(Received 22 June 2015; published 20 October 2015)

Direct evidence of excitation of the $5p_{3/2} \rightarrow 6p_{3/2}$ electric-dipole-forbidden transition in atomic rubidium is presented. The experiments were performed in a room-temperature rubidium cell with continuous-wave external cavity diode lasers. Optical-optical double-resonance spectroscopy with counterpropagating beams allows the detection of the nondipole transition free of Doppler broadening. The $5p_{3/2}$ state is prepared by excitation with a laser locked to the maximum F cyclic transition of the D_2 line, and the forbidden transition is produced by excitation with a 911 nm laser. Production of the forbidden transition is monitored by detection of the 420 nm fluorescence that results from decay of the $6p_{3/2}$ state. Spectra with three narrow lines (≈13 MHz FWHM) with the characteristic $F-1$, F, and $F+1$ splitting of the $6p_{3/2}$ hyperfine structure in both rubidium isotopes were obtained. The results are in very good agreement with a direct calculation that takes into account the $5s \rightarrow 5p_{3/2}$ preparation dynamics, the $5p_{3/2} \rightarrow 6p_{3/2}$ nondipole excitation geometry, and the $6p_{3/2} \rightarrow 5s_{1/2}$ decay. The comparison also shows that the electric-dipole-forbidden transition is a very sensitive probe of the preparation dynamics.

DOI: 10.1103/PhysRevA.92.042511 PACS number(s): 32.70.Cs, 32.70.Fw

I. INTRODUCTION

While the electric dipole approximation is a cornerstone in the study of the interaction between optical radiation fields and atoms, transitions induced by optical fields beyond this approximation have also become important tools in atomic structure calculations. These so-called "forbidden transitions" have been traditionally used in astrophysical and plasma studies [1]. They now play a fundamental role in metrology [2] and have also been used in experiments testing parity nonconserving interactions in atoms [3].

In early studies of forbidden transitions, Sayer *et al.* [4] determined transition probabilities of electric quadrupole (E_2) transitions using a tungsten lamp. The first direct observation of electric quadrupole effects in multiphoton ionization dates back to the work of Lambropoulos *et al.* [5]. Electric-dipole-forbidden transitions were exploited in three-wave-mixing experiments for optical sum and difference frequency generation in Ref. [6].

The use of intense continuous-wave or pulsed laser sources has facilitated the observation of weak absorption lines. For instance, Guéna *et al.* [7] recorded evidence of the highly forbidden $6s_{1/2} \rightarrow 7s_{1/2}$ transition by detecting a fluorescence inhibition in a three-level system driven by two cw lasers in a heated caesium vapor. More recently, Tojo *et al.* [8] reported a determination of the oscillator strength of a E_2 transition with a temperature-controlled cell and an external cavity diode laser. Also, the study of strongly forbidden $J=0 \rightarrow J=0$ transitions via single-photon excitation is presented in Ref. [9]. Excitation of forbidden transitions involving states with nonzero angular momentum in alkali-metal atoms have also been studied over the past few years [10–14]. The coherent mixing of waves is theoretically studied in Ref. [10] for $n_1\,^2p \rightarrow n_2\,^2p$ transitions. The excitation of the $5p \rightarrow 8p$ forbidden transition in thermal rubidium atoms was produced with a sequence of pulsed lasers by Bayram *et al.* [11] and the same transition is observed in ultracold rubidium atoms with narrowband cw lasers in Ref. [13].

The experiment with ultracold atoms [13] allowed resolution of the atomic hyperfine structure and conclusively determined that the magnetic dipole contribution to this transition was negligible. Other experiments with dipole-forbidden transitions and ultracold alkali-metal atoms include the measurement of the $3p \rightarrow 4p$ transition in sodium [12] and also the $5s \rightarrow nd$ transitions in rubidium [14]. Recently, experiments performed in atomic vapor nanocells with a half-wavelength thickness and an applied magnetic field demonstrated a strong enhancement of the probabilities of forbidden transitions [15].

In this article we present experimental observations of the $5p_{3/2} \rightarrow 6p_{3/2}$ electric-dipole-forbidden transition using external cavity diode lasers (ECDL) in atomic rubidium at room temperature. We were able to resolve the hyperfine structure of the $6p_{3/2}$ state. Even though the results presented here pertain a $p \rightarrow p$ transition in atomic rubidium, our results clearly indicate that similar experiments can be performed with the other alkali-metal atoms. This is in agreement with the observation in Ref. [12] that moderate cw laser powers could be used to excite the $np \rightarrow (n+1)p$ forbidden transition in any of the alkali metals. The data are compared with the results of a calculation that considers three independent steps, namely, state preparation, nondipole excitation, and decay of the $6p_{3/2}$ levels, where the first and third steps are dipole transitions, whereas the nondipole excitation is an electric quadrupole transition.

*ferama@nucleares.unam.mx
†jimenez@nucleares.unam.mx

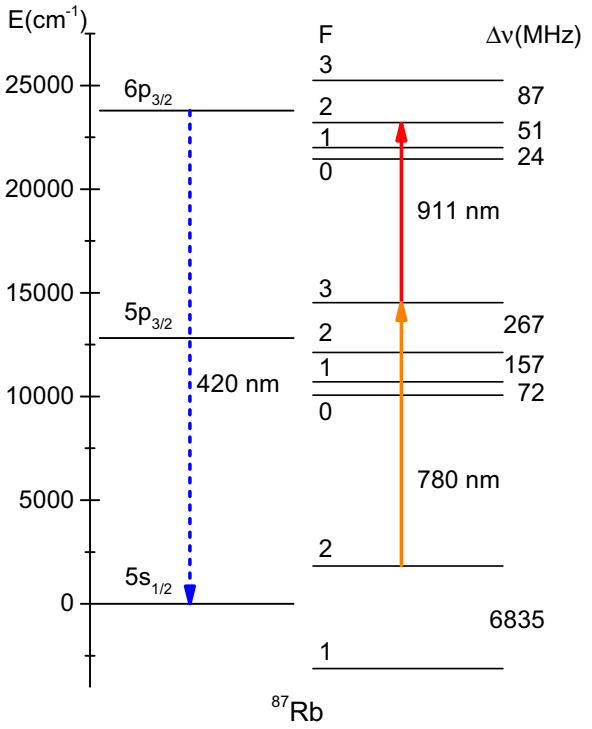

FIG. 1. (Color online) Energy levels of ^{87}Rb. The left panel includes the fine structure. The hyperfine structure is shown to the right. Note that the frequency scale changes for the hyperfine structure of each state.

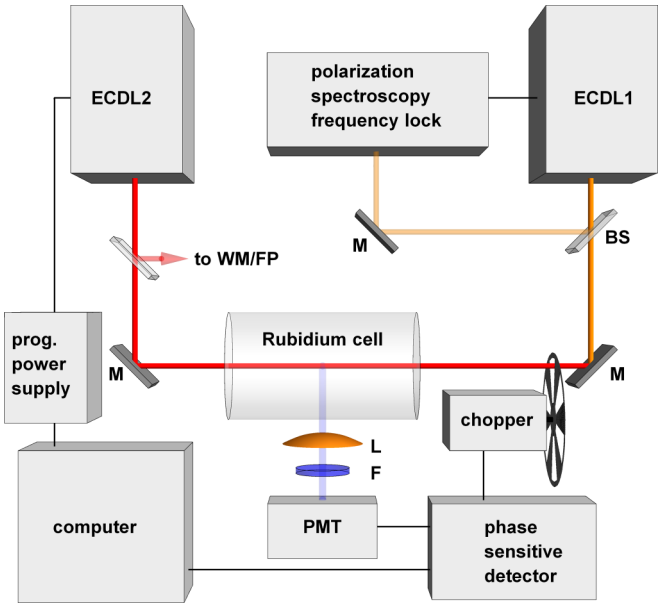

FIG. 2. (Color online) Experimental setup for polarized velocity selective spectroscopy. ECDL: external cavity diode laser; PMT: photomultiplier tube; M: mirror; BS: beam splitter; L: lens system; F: 420 nm interference filter. A small part of the 911 nm beam is sent to a wave meter (WM) and a 1.5 GHz Fabry-Pérot interferometer (FP).

II. EXPERIMENTAL SETUP

Figure 1 shows an energy-level diagram, where the total angular momentum quantum numbers and the hyperfine splittings correspond to ^{87}Rb. A similar figure, with different values of F and hyperfine splittings, is obtained for ^{85}Rb. In the experiment a laser in resonance with the $5s \rightarrow 5p_{3/2}$ transition at 780 nm (D_2 line) is used to prepare atoms in the $5p_{3/2}$ state. A second laser beam at 911 nm is used to produce the $5p_{3/2} \rightarrow 6p_{3/2}$ electric-dipole-forbidden transition. We detect this excitation channel because atoms in the $6p_{3/2}$ state have a significant probability of decaying directly into the $5s$ ground state by emission of a 420 nm photon.

The experimental setup is shown in Fig. 2. Home-built external cavity diode lasers (ECDL) provide the 780 and 911 nm photon beams. Both lasers were built after the design of Refs. [16,17], adapted to the emission wavelengths. ECDL1 operates at the frequency of the D_2 transition in atomic rubidium (780 nm). It has an emission bandwidth of less than 6 MHz. Its frequency can be locked to the Doppler-free cyclic transition of either of the rubidium isotopes [18,19]. ECDL2 uses a laser diode with a nominal emission wavelength of 915 nm [20]. The external cavity configuration was designed and built to tune the emission of this laser to 911 nm. It operates in a single mode and can be tuned across mode-hop free regions of $\approx$3 GHz. The bandwidth of the laser is narrower than the 7.5 MHz resolution of a confocal scanning Fabry-Pérot interferometer (Thorlabs, 1.5 GHz FSR, SA200-8B). Under normal operation conditions one obtains up to 100 mW of single-mode laser power at the output of the external cavity. Both beams are linearly polarized with parallel electric-field vectors, and counterpropagate along a rubidium cell at room temperature. The production of the electric-dipole-forbidden transition is monitored by detecting the 420 nm fluorescence that results from the direct decay into the $5s$ ground state. These blue photons are collected by a lens system that focuses them into the cathode of a photomultiplier tube (PMT). A bandpass filter centered at 420 nm is placed in front of the PMT window. In the experimental setup the detection direction is perpendicular to the linear polarization direction of both laser beams, and also perpendicular to their propagation direction. A chopper is used to modulate the incidence of the preparation beam with a frequency of 800 Hz. The amplified PMT current signal and the chopper reference frequency signal are sent to a phase sensitive detector whose voltage output is read in a computer interface. This interface also controls a programmable power supply that is used to scan the frequency of ECDL2. An electric-dipole-forbidden spectrum is the in-phase PMT signal as a function of the voltage applied to the frequency scan of ECDL2. A wave meter with a 0.05 nm resolution is used for the initial tuning of ECDL2. The Fabry-Pérot interferometer mentioned above is used to monitor the single-mode operation of ECDL2, and it also provides a coarse frequency scale.

Both laser beams were collimated and produced elliptical cylinders along the 7.5-cm-long rubidium cell. The ECDL1 beam profile was a 4.9 mm $\times$ 2.4 mm ellipse and that of ECDL2 was a 4.5 mm $\times$ 2.3 mm ellipse. Both beams overlap inside the rubidium cell. For the 911 nm beam we used the maximum available power of 100 mW, which results in an average intensity of 12.3 kW m^{-2}. The fluorescence lines can be broadened by the power of the 780 nm preparation beam. We therefore decided to use 100 μW of power. This puts

its average intensity at 10.7 W m^{-2}, below the 16.46 W m^{-2} saturation intensity for the D_2 transition [21].

In either rubidium isotope, the $5s_{1/2}$ hyperfine splitting is larger than the D_2 Doppler width at room temperature. Therefore, the frequency of the preparation photons at 780 nm has been used to determine the initial hyperfine state of the three-step excitation sequence. We used polarization spectroscopy [18,19] to lock the frequency of the preparation beam to the Doppler free $F \rightarrow F+1$ cyclic transition ($F = 2$ in ^{87}Rb or $F = 3$ in ^{85}Rb). The 911 nm laser has been used to excite the $5p_{3/2} \rightarrow 6p_{3/2}$ electric-dipole-forbidden transition. By sending it in a counterpropagating configuration one can perform a Doppler free excitation into the hyperfine states of the $6p_{3/2}$ manifold [22]. For zero velocity atoms the excitation sequence is $F_1 = F \rightarrow F_2 = F+1 \rightarrow F_3$. Direct use of the electric quadrupole selection rules ($\Delta F = 0, \pm 1, \pm 2$) results in $F_3 = 1$, 2, and 3 for ^{87}Rb and $F_3 = 2$, 3, and 4 for ^{85}Rb. For each isotope one therefore expects a triplet with the frequency splitting of the well-known hyperfine structure of the $6p_{3/2}$ state [23]. These splittings were used for the frequency calibration of the dipole-forbidden spectra.

III. CALCULATION OF RELATIVE LINE INTENSITIES

The relative intensities of the emission that follows the electric-dipole-forbidden excitation have been calculated. We found that the experimental results for these intensities are properly described assuming that (i) the system can be described in terms of three sequential steps (preparation $5s \rightarrow 5p_{3/2}$, electric quadrupole excitation $5p_{3/2} \rightarrow 6p_{3/2}$, and decay $6p_{3/2} \rightarrow 5s$) and (ii) the rate equation approximation is valid for the description of the first step. The assumption (i) is based on the fact that the forbidden excitation is very weak compared to the transitions of the preparation step, so that the modification of the population of the $5p_{3/2}$ states due to both the electric quadrupole excitation and the subsequent electric dipole decay can be neglected in a first analysis.

Under these assumptions, the probability to observe a 420 nm photon resulting from the decay of the $|6p_{3/2}F_3\rangle$ hyperfine states is given by

$$P(F_3) = \sum_{M_2,M_3,F_1',M_1',\lambda} \sigma(F_2,M_2)|\langle 5p_{3/2}F_2M_2|T|6p_{3/2}F_3M_3\rangle|^2 \times |\langle 6p_{3/2}F_3M_3|D_\lambda|5s_{1/2}F_1'M_1'\rangle|^2. \quad (1)$$

Here $\sigma(F_2,M_2)$ is the population of the $|5p_{3/2}F_2M_2\rangle$ prepared by the 780 nm laser, T is the nondipole transition operator, and D_λ is the $6p_{3/2} \rightarrow 5s_{1/2}$ electric dipole decay operator associated to the polarization λ. The sum is performed over all projections of total angular momenta of the initial M_2 and final M_3 states of the nondipole transition, the angular momenta of the final $5s_{1/2}$ hyperfine states (F_1', M_1'), and also over two orthogonal polarization directions λ. The value of the total angular momentum of the intermediate state F_2 corresponds to the $F \rightarrow F+1$ cyclic transition of the D_2 preparation step.

The geometry of the experiment that is used in the calculation is the following (Fig. 3). The preparation and nondipole beams counterpropagate along the x axis. They are both linearly polarized, with parallel electric-field vectors. We take this polarization direction as the z axis. Finally, the 420 nm fluorescence is detected along the y axis.

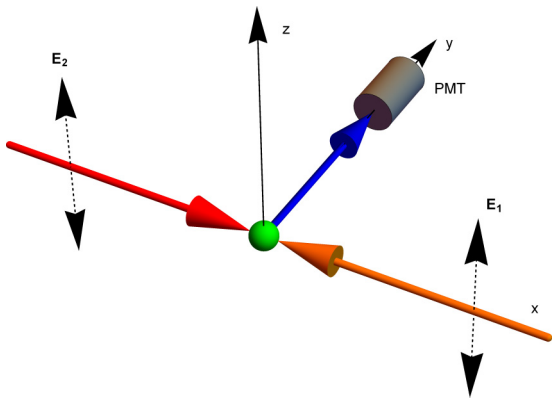

FIG. 3. (Color online) Geometry used in the calculation. The preparation (780 nm) and the forbidden excitation (911 nm) beams propagate respectively in the negative and positive directions of the x axis with parallel linear polarizations $\mathbf{E_1}$ and $\mathbf{E_2}$ directed along the z axis. The detection of the fluorescence is performed by the PMT in the positive direction of the y axis.

The first step is then the calculation of the alignment of the $5p_{3/2}F_2 = F+1$ state induced by the preparation laser. This establishes the relative populations $\sigma(F_2,M_2)$ of the magnetic sublevels [19], which were calculated using the rate equation approximation taking into account the transit time T_{trans} of the atoms across the preparation beam [19]. Einstein rate equations for the F and $F_2 = F+1$ states in the cyclic transition [say, $F_1 = 2(3)$ and $F_2 = 3(4)$ for ^{87}Rb (^{85}Rb)] with all the magnetic projections M read

$$\frac{dN_{M_i}}{dt} = \rho B_{M_i}^{M_j}\left(N_{M_j} - N_{M_i}\right) + \sum_{M_j} A_{M_i}^{M_j} N_{M_j}, \quad (2)$$

$$\frac{dN_{M_j}}{dt} = -\rho B_{M_i}^{M_j}\left(N_{M_j} - N_{M_i}\right) - \sum_{M_i} A_{M_i}^{M_j} N_{M_j}. \quad (3)$$

Equation (2) describes the changes on the population of the lower F, M_i states so that the sum runs over all the possible upper states F_2, M_j that can decay spontaneously to the M_i state with an Einstein coefficient $A_{M_i}^{M_j}$; the stimulated transitions involve the Einstein coefficients $B_{M_i}^{M_j}$ multiplied by the radiation energy density ρ. The second equation, Eq. (3), describes the changes on the population of the upper F, M_j states. In it, the sum now runs over all the lower M_i states coupled by spontaneous emission. Clearly, Eq. (2) is the negative of Eq. (3) establishing a conservation of population that is approximately valid under the experimental conditions since the second step corresponds to the much less probable forbidden transition.

The Euler method was used to solve the differential equations (2) and (3) using temporal evolutions corresponding to several values of ρ and a time $T_{\text{trans}} \sim 10\ \mu$s, which corresponds to the mean transit of thermal atoms ($T \sim 300$ K) through the laser beams used in the experiment. The time

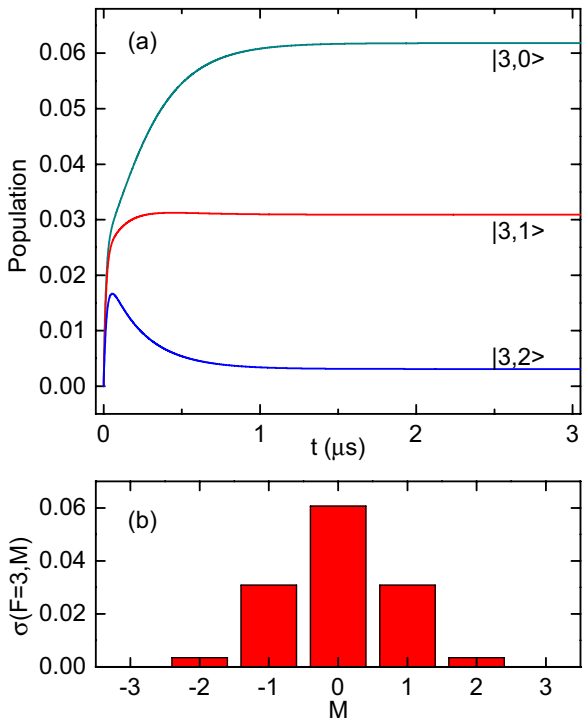

FIG. 4. (Color online) (a) Temporal evolution of the populations of the $5p_{3/2}$ $F = 3$ M_F magnetic sublevels for ^{87}Rb; (b) time average of these $5p_{3/2}$ magnetic state populations $[\sigma(F = 3, M_F)]$ integrated over a time period of 10 μs.

average of the population $N_M(t)$ yields the $\sigma(F_2, M_2)$ value,

$$\sigma(F_2, M_2) = \frac{1}{T_{\text{trans}}} \int_0^{T_{\text{trans}}} N_M(t) dt. \tag{4}$$

Figure 4(a) illustrates the temporal evolution for the population of the $|5P_{3/2}, F_2 = 3M\rangle$ magnetic projection states for ^{87}Rb. The preparation beam is linearly polarized with an energy density ρ corresponding to an intensity $I = 0.65 I_0$, where I_0 is the saturation intensity for rubidium D_2 line, and its frequency is resonant to the $F_1 = 2 \rightarrow F_2 = 3$ cyclic transition. The behavior of the negative M levels is identical to that of the positive M levels. The selection rule for linearly polarized light $\Delta M = 0$ prevents excitation into the $M = \pm 3$ sublevels. For this preparation intensity the steady-state population of all magnetic sublevels is reached within the first two microseconds. For $M = 0$ and ± 1 the steady state is asymptotically reached from below, while for $M = \pm 2$ there is a population maximum for very short excitation times, and the steady state is reached from above. Figure 4(b) shows the $\sigma(F_2 = 3, M_2)$ obtained taking the time average of the populations over a transit time of 10 μs. These are the available populations that could be excited by the quadrupole electric transition. It can be observed that the population is maximum for the magnetic state $M_2 = 0$, but that there are significant contributions from the $M = \pm 1$ and $M = \pm 2$ states. Qualitatively similar time evolution curves and population distributions are found for different values of the energy density of the preparation laser. The time to achieve the steady state is reduced for higher values of ρ, and the corresponding asymptotic population values are larger. It is interesting, however, that the ratios $\sigma(3, M)/\Sigma_M \sigma(3, M)$ remain almost constant for $0.1 \leqslant I/I_0 \leqslant 1.0$. Equivalent results were obtained for ^{85}Rb.

The second step corresponds to the calculation of the $5p_{3/2} \rightarrow 6p_{3/2}$ nondipole excitation. This transition could arise from electric quadrupole and magnetic dipole couplings of the atom to the light field. Previous studies of the $5p \rightarrow 8p$ dipole-forbidden transition in cold rubidium atoms [13] showed no significant contribution from magnetic dipole couplings; the ultimate reason was that a radiative $M1$ transition between states of the same parity but with orthogonal spatial wave functions is highly forbidden; its description in general requires taking into account subtle relativistic effects. There is no reason to expect a different scenario in our experimental setup. Therefore, in the present calculation, we restricted our study to the electric quadrupole transition operator T. Since the nondipole beam counterpropagates to the dipole beam along the x axis, and it is also linearly polarized in the z direction with an electric-field amplitude E_{2_0}, the relevant component of the electric quadrupole tensor operator is

$$T = -eE_{2_0} z(ik_2 x), \tag{5}$$

which is written in terms of the components of the irreducible tensor operators of rank two,

$$T = -eE_{2_0} k_2 r^2 \frac{-Y_{2,1} + Y_{2,-1}}{\sqrt{2}}. \tag{6}$$

The Wigner-Eckart theorem then gives the transition matrix element

$$\begin{aligned}
&\langle 5p_{3/2} F_2 M_2 | T | 6p_{3/2} F_3 M_3 \rangle \\
&= (-1)^{F_2 - M_2} \sqrt{\frac{(2F_2 + 1)(2F_3 + 1)}{2}} \begin{Bmatrix} J_3 & F_3 & I \\ F_2 & J_2 & 2 \end{Bmatrix} \\
&\times \left[-\begin{pmatrix} F_2 & 2 & F_3 \\ -M_2 & 1 & M_3 \end{pmatrix} + \begin{pmatrix} F_2 & 2 & F_3 \\ -M_2 & -1 & M_3 \end{pmatrix} \right] \\
&\times \langle 5p_{3/2} \| T \| 6p_{3/2} \rangle,
\end{aligned} \tag{7}$$

where the terms in parentheses are Wigner 3-j symbols, the curly bracket is a 6-j symbol, I is the nuclear spin, and $\langle 5p_{3/2} \| T \| 6p_{3/2} \rangle$ is the reduced matrix element. For this geometry the selection rules for the magnetic quantum numbers are

$$\Delta M = \pm 1. \tag{8}$$

Finally, the $6p \rightarrow 5s$ decay was observed along the y axis, with no polarization selection. Therefore, for calculating the measured relative decay rates we took incoherent sums of the $D_1 = x$ and $D_2 = z$ electric dipole operators.

The resulting intensities of the triplet F_3 lines, through the Wigner-Eckart theorem, have a common factor that is the product of squares of reduced matrix elements of the electric quadrupole transition and the electric dipole transitions $\langle 6p_{3/2} \| D \| 5s_{1/2} \rangle$. These factors cancel out for relative line intensities, which have been directly compared with the experimental data. The calculation indicates that geometrical effects in the $6p \rightarrow 5s$ decay play a minor role (less than 3%) in the relative intensities. On the other hand, the relative peak intensities strongly depend on the populations of the $5p_{3/2}$ magnetic sublevels produced in the preparation state. Therefore, the electric quadrupole transition is at the same

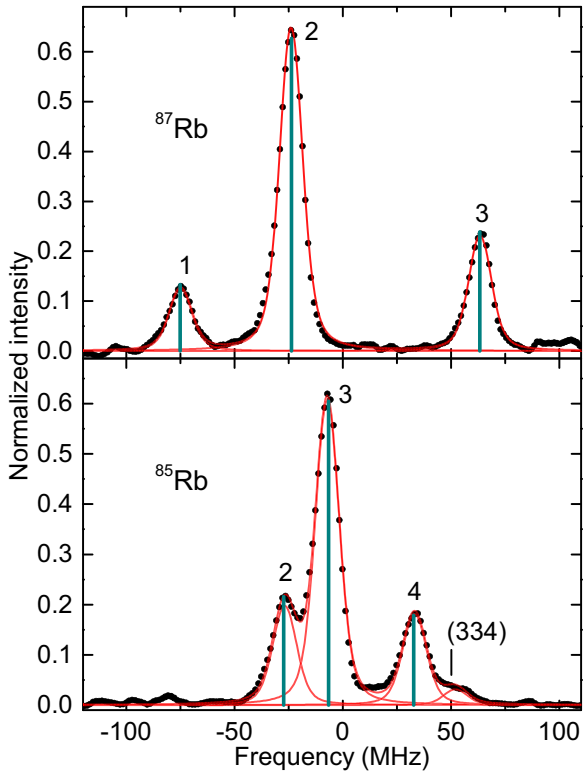

FIG. 5. (Color online) Fluorescence emission spectra. Dots: experimental data; continuous lines: result of fitting Voigt profiles to each line. The numeric labels indicate the F value of the $6p_{3/2}$ hyperfine state. The velocity selected transition in ^{85}Rb is indicated by the parentheses with the F values of the excitation chain. The vertical bars give the position and calculated relative intensity of each hyperfine state.

time a sensitive and nonperturbing probe of the preparation dynamics of the $5p_{3/2}M_2$ magnetic sublevels.

IV. RESULTS: COMPARISON BETWEEN EXPERIMENT AND THEORY

Figure 5 shows typical spectra of the fluorescence signal recorded as the frequency of the 911 nm laser was scanned. The original horizontal scale is the voltage applied to the ECDL2 piezo. A coarse frequency equivalence is obtained with the Fabry-Pérot interferometer. The least-squares fits of independent Voigt profiles [24] shown in the plot were performed for each spectrum. The center and height of each peak was varied independently, whilst the widths (Gaussian and Lorentzian) were the same for all peaks. The differences between peak centers were then fit to the known $6p_{3/2}$ hyperfine splittings [23]. Finally, the zero in frequency was shifted to the center of gravity of the $6p_{3/2}$ hyperfine manifold common to both isotopes [23]. After this calibration the resulting total linewidth for both isotopes is $\Gamma = 12.9 \pm 0.2$ MHz (FWHM).

For both isotopes we observe the expected three lines that result from the excitation sequence $5s_{1/2}F \rightarrow 5p_{3/2}F + 1 \rightarrow 6p_{3/2}F_3$ ($F_3 = F - 1$, F, and $F + 1$) for zero velocity atoms. Also, the splittings of the triplets correspond to the known frequency separation between the $6p_{3/2}F_3$ hyperfine states of each isotope [23]. However, other groups of atoms, with nonzero velocity projections, are also excited by the preparation laser. For these groups the Doppler shift of the counterpropagating 911 nm laser only partially compensates the Doppler shift of the preparation beam, and the dipole-forbidden transitions appear at frequencies different to the ones obtained with the maximum F preparation. The strongest of these velocity-selected nondipole transitions results from the $F \rightarrow F \rightarrow F + 1$ excitation chain ($2 \rightarrow 2 \rightarrow 3$ in ^{87}Rb and $3 \rightarrow 3 \rightarrow 4$ in ^{85}Rb). In ^{85}Rb there is a clear indication of a shoulder $\approx$19 MHz above the $F = 4$ peak, in good agreement with position of the velocity selected transition that is expected to appear 16.4 MHz above the $3 \rightarrow 3 \rightarrow 4$ excitation. No evidence of the corresponding $2 \rightarrow 2 \rightarrow 3$ transition is found in the ^{87}Rb spectrum. This transition is expected to occur 37 MHz above the $F_3 = 3$ line in Fig. 5.

The fit also gives information about the relative intensity of the hyperfine lines. For ^{85}Rb the relative intensities are 20%, 62%, and 18%, while for ^{87}Rb they are 12%, 65%, and 23%. The calculated relative line intensities are 22%, 60%, and 18% for ^{85}Rb and 13%, 63%, and 24% for ^{87}Rb, in very good agreement with the measured values. No variation of these ratios was found for values of the preparation laser power between 10 and 100 μW. This is in agreement with the calculation that also predicts no significant change of the intensity ratios in this range of preparation laser intensities.

The intensity of the velocity selected peak in ^{85}Rb ($3 \rightarrow 3 \rightarrow 4$) is 3.2% of the sum of intensities of the other three peaks. In the calculation the electric quadrupole transition probability for this line is comparable to the ones in the zero velocity triplet. The reduction of its intensity is explained in terms of optical pumping effects that effectively move the $F_2 = 3$ population into the $F_1 = F - 1 = 2$ dark state.

V. CONCLUSIONS

In summary, direct evidence of the $5p_{3/2} \rightarrow 6p_{3/2}$ electric-dipole-forbidden excitation using ECLD in atomic rubidium at room temperature was observed. Efficient detection of the fluorescence that follows the Doppler-free optical-optical excitation allowed resolution of the $6p_{3/2}$ hyperfine structure. Our results confirm that the $5p_{3/2} \rightarrow 6p_{3/2}$ excitation is the result of an electric quadrupole transition. A simple calculation using a sequential two-step excitation and one-step decay is in very good agreement with the experiment. This electric-dipole-forbidden transition is a very sensitive probe of the dynamics of the $5s \rightarrow 5p_{3/2}$ preparation step.

ACKNOWLEDGMENTS

We thank J. Rangel for his help in the construction of the diode laser. This work was supported by DGAPA-UNAM, Mexico, under Projects PAPIIT No. IN116309, No. IN110812, and No. IA101012, by CONACyT, Mexico, under Basic Research Project No. 44986, and National Laboratory Project No. LN260704.

[1] E. Biémont and C. J. Zeippen, Probabilities for forbidden transitions in atoms and ions: 1989-1995. A commented bibliography, Phys. Scr., **T65**, 192 (1996).

[2] R. van Rooij, J. S. Borbely, J. Simonet, M. D. Hoogerland, K. S. E. Eikema, R. A. Rozendaal, and W. Vassen, Frequency metrology in quantum degenerate helium: Direct measurement of the $2\,^3S_1 \rightarrow 2\,^1S_0$ transition, Science **333**, 196 (2011).

[3] M.-A. Bouchiat and C. Bouchiat, Parity violation in atoms, Rep. Prog. Phys. **60**, 1351 (1997).

[4] B. Sayer, R. Wang, J. C. Jeannet, and M. Sassi, Absorption measurements of quadrupole transition probabilities 6s-nD in caesium vapour, J. Phys. B **4**, L20 (1971).

[5] M. Lambropoulos, S. E. Moody, S. J. Smith, and W. C. Lineberger, Observation of Electric Quadrupole Transitions in Multiphoton Ionization, Phys. Rev. Lett. **35**, 159 (1975).

[6] A. Flusberg, T. Mossberg, and S. R. Hartmann, Optical Difference-Frequency Generation in Atomic Thallium Vapor, Phys. Rev. Lett. **38**, 59 (1977); Optical Sum-Frequency-Generation Interference in Atomic Sodium Vapor, **38**, 694 (1977).

[7] J. Guéna, M. Lintz, P. Jacquier, L. Pottier, and M. Bouchiat, Doppler-free inhibited fluorescence spectroscopy of a forbidden three-level system, Opt. Commun. **62**, 97 (1987).

[8] S. Tojo, T. Fujimoto, and M. Hasuo, Precision measurement of the oscillator strength of the cesium $6\,^2S_{1/2} \rightarrow 5\,^2D_{5/2}$ electric quadrupole transition in propagating and evanescent wave fields, Phys. Rev. A **71**, 012507 (2005).

[9] A. V. Taichenachev, V. I. Yudin, C. W. Oates, C. W. Hoyt, Z. W. Barber, and L. Hollberg, Magnetic Field-Induced Spectroscopy of Forbidden Optical Transitions with Application to Lattice-Based Optical Atomic Clocks, Phys. Rev. Lett. **96**, 083001 (2006); Z. W. Barber, C. W. Hoyt, C. W. Oates, L. Hollberg, A. V. Taichenachev, and V. I. Yudin, Direct Excitation of the Forbidden Clock Transition in Neutral ^{174}Yb Atoms Confined to an Optical Lattice, *ibid.* **96**, 083002 (2006).

[10] P. V. Mironova, V. D. Ovsiannikov, and V. V. Tchernoushkine, Interference of E2 and M1 $n_1\,^2P - n_2\,^2P$ transition amplitudes in steady-field-induced coherent mixing of two resonant waves on atoms, J. Phys. B **38**, 2467 (2005); E2/M1 amplitude ratio in dipole-forbidden transitions of alkali atoms from two-wave mixing, Laser Phys. **15**, 492 (2005).

[11] S. B. Bayram, M. D. Havey, D. V. Kupriyanov, and I. M. Sokolov, Anomalous depolarization of the $5p\,^2P_{3/2} \rightarrow 8p\,^2P_{j'}$ transitions in atomic ^{87}Rb, Phys. Rev. A **62**, 012503 (2000).

[12] M. Bhattacharya, C. Haimberger, and N. P. Bigelow, Forbidden Transitions in a Magnetooptical Trap, Phys. Rev. Lett. **91**, 213004 (2003).

[13] R. Pires, M. Ascoli, E. E. Eyler, P. L. Gould, and A. Derevianko, Upper limit on the magnetic dipole contribution to the 5p-8p transition in Rb by use of ultracold atom spectroscopy, Phys. Rev. A **80**, 062502 (2009).

[14] D. Tong, S. M. Farooqi, E. G. M. van Kempen, Z. Pavlovic, J. Stanojevic, R. Côté, E. E. Eyler, and P. L. Gould, Observation of electric quadrupole transitions to Rydberg *nd* states of ultracold rubidium atoms, Phys. Rev. A **79**, 052509 (2009).

[15] G. Hakhumyan, C. Leroy, R. Mirzoyan, Y. Pashayan-Leroy, and D. Sarkisyan, Study of "forbidden" atomic transitions on D_2 line using Rb nano-cell placed in external magnetic field, Eur. Phys. J. D **66**, 119 (2012); A. Sargsyan, A. Tonoyan, G. Hakhumyan, A. Papoyan, E. Mariotti, and D. Sarkisyan, Giant modification of atomic transition probabilities induced by a magnetic field: Forbidden transitions become predominant, Laser Phys. Lett. **11**, 055701 (2014).

[16] A. S. Arnold, J. S. Wilson, and M. G. Boshier, A simple extended-cavity diode laser, Rev. Sci. Instrum. **69**, 1236 (1998).

[17] C. J. Hawthorn, K. P. Weber, and R. E. Scholten, Littrow configuration tunable external cavity diode laser with fixed direction output beam, Rev. Sci. Instrum. **72**, 4477 (2001).

[18] C. P. Pearman, C. S. Adams, S. G. Cox, P. F. Griffin, D. A. Smith, and I. G. Hughes, Polarization spectroscopy of a closed atomic transition: Applications to laser frequency locking, J. Phys. B **35**, 5141 (2002).

[19] M. L. Harris, C. S. Adams, S. L. Cornish, I. C. McLeod, E. Tarleton, and I. G. Hughes, Polarization spectroscopy in rubidium and cesium, Phys. Rev. A **73**, 062509 (2006).

[20] Axcel Photonics. 905/915 nm Single-Mode Laser Diodes, 200 mW Series, Product No. M9-915-0200-s50.

[21] H. J. Metcalf and P. van der Straten, *Laser Cooling and Trapping* (Springer, New York, 1999).

[22] M. Kaminsky, R. T. Hawkins, F. V. Kowalski, and A. L. Schawlow, Identification of Absorption Lines by Modulated Lower-Level Population: Spectrum of Na_2, Phys. Rev. Lett. **36**, 671 (1976).

[23] E. Arimondo, M. Inguscio, and P. Violino, Experimental determinations of the hyperfine structure in the alkali atoms, Rev. Mod. Phys. **49**, 31 (1977).

[24] A. Corney, *Atomic and Laser Spectroscopy*, Oxford Classic Texts in the Physical Sciences (Oxford University Press, Oxford, 2006).